Heliyon

*Received:*
7 December 2018
*Revised:*
20 March 2019
*Accepted:*
11 April 2019

Cite as: S. S. Balabanov, S. V. Filofeev, M. G. Ivanov, E. G. Kalinina, D. K. Kuznetsov, D. A. Permin, E. Y. Rostokina. Self-propagating high-temperature synthesis of $(Ho_{1-x}La_x)_2O_3$ nanopowders for magneto-optical ceramics. Heliyon 5 (2019) e01519. doi: 10.1016/j.heliyon.2019.e01519

# Self-propagating high-temperature synthesis of $(Ho_{1-x}La_x)_2O_3$ nanopowders for magneto-optical ceramics

**S. S. Balabanov [a], S. V. Filofeev [a], M. G. Ivanov [a,b,c,*], E. G. Kalinina [b,c], D. K. Kuznetsov [c], D. A. Permin [a], E. Y. Rostokina [a]**

[a] *G.G. Devyatykh Institute of Chemistry of High-Purity Substances, Russian Academy of Sciences, 49 Tropinin Str., Nizhny Novgorod, Russia*

[b] *Institute of Electrophysics, Ural Branch of Russian Academy of Sciences, 106 Amundsen Str., Ekaterinburg, 620016, Russia*

[c] *Ural Federal University, 19 Mira Avenue, Ekaterinburg, 620002, Russia*

[*] Corresponding author.

E-mail address: max@iep.uran.ru (M.G. Ivanov).

## Abstract

Weakly agglomerated nanoparticles of $(Ho_{1-x}La_x)_2O_3$ solid solutions were synthesized with the help of a self-propagating high-temperature synthesis (SHS). The nanopowders were studied by a simultaneous thermal analysis (TG-DSC), X-ray diffraction (XRD), BET and FT-IR spectroscopy methods. Changes of the particles morphology after annealing at different temperatures and ball milling were investigated by a scanning electron microscopy (SEM) and a dynamic light scattering (DLS) method. It was found that annealing at a temperature of 900 °C in air and ball milling of the SHS nanopowders allow obtaining rounded shape particles with a mean diameter of about 20 nm and C-type cubic crystal structure. Up to 10 mol.% of the lanthana was shown to dissolve in the holmium oxide nanoparticles.

Keywords: Nanotechnology, Mechanical engineering, Materials science

https://doi.org/10.1016/j.heliyon.2019.e01519

## 1. Introduction

Up to now, most of Faraday isolators and rotators operating in a near-IR range are made of terbium compounds: terbium-gallium garnet (TGG), terbium-aluminum garnet and terbium-borogermanate glasses. Neat $Tb_2O_3$ would be an excellent material for these applications due to the highest content of $Tb^{3+}$ ions, but the material undergoes a phase transformation at temperatures of about 1600−1700 °C which, along with polyvalence of the terbium, are significant obstructions to a fabrication of the material with high transparency. Besides, strong absorption of IR radiation by the $Tb^{3+}$ ions at the wavelengths above 1.5 μm limits the use of the terbium based materials in the middle IR range [1, 2].

Progress in the development of the elements for the Faraday isolators can be achieved by using a material, which contains the highest concentration of paramagnetic ions with properties similar to $Tb^{3+}$. Potentially, such materials can be other oxides of rare-earth (RE) elements. For example, it has been recently demonstrated that holmium oxide ceramics, in comparison with the TGG, have 1.3 times greater value of the Verdet constant [3, 4]. On the other hand, the rare-earth sesquioxides single crystals are extremely difficult to grow with common techniques, since most of the oxides undergo phase transformations upon heating − cooling process, which could lead to damage of the crystals [5]. Ceramic approach to the fabrication of polycrystalline sesquioxides in recent years has been noted as the most promising one, since the ceramics sintering temperature is much lower than the material melting point, and on its basis, a number of optical ceramics with unique characteristics have already been made [2, 6, 7]. As is well-known, the ceramic technology has three important steps: powder synthesis, compacting and sintering, and a key stage is the synthesis of the nanopowders [8, 9, 10, 11]. To obtain the transparent ceramics, the fabrication of highly dispersed nanopowders with a low agglomeration degree is essential [12, 13]. The nano-size requirement is due to the high activity of such powders needed to sinter fully dense ceramics. The low agglomeration is immensely important for uniform packing of the nanoparticles in a green body since the particles agglomerates lead to the appearance of pores in the ceramics upon sintering, which is exceedingly harmful to the optical quality due to light scattering [14].

To obtain the nanopowders of both pure and solid solution rare-earth sesquioxides, which meet these requirements, a method of self-propagating high-temperature synthesis (SHS) was successfully applied [7, 15, 16, 17, 18, 19, 20]. Comparing to a commonly used co-precipitation technique [20], the SHS allows obtaining weakly agglomerated nanopowders within one stage (there's no need for washing, drying, etc.). Besides, in comparison with other techniques, such as laser synthesis, for instance [9, 14, 21, 22, 23, 24], the method gives a chance to get a chemical composition of the synthesized powders with a sufficient accuracy


https://doi.org/10.1016/j.heliyon.2019.e01519

[19]. Another important issue in the fabrication of the optical ceramics is the type and concentration of sintering aids, which helps the material to form the desired faultless microstructure [25]. One of the most effective sintering aids for the sesquioxides is lanthana, which was proved to assist both phase transition sintering at high temperature [26] and lower temperature sintering [24]. At a concentration of 5−10 mol.% the $La_2O_3$ were proved to help sintering high-quality $Y_2O_3$ [9, 17, 20, 21, 27], $Dy_2O_3$ [6, 7] and $Lu_2O_3$ [25, 28] optical ceramics. Concerning an effect of the aid on the ceramics densification, a possible phase transformation at the sintering temperatures can provide a significant amount of defects and accelerate mass transfer. Such an approach demonstrated its effectiveness in the case of YAG transparent ceramics [28, 29, 30, 31, 32, 33]. On the other hand, relatively low transition temperature at phase equilibrium point in the $La_2O_3$-$Ho_2O_3$ system, when the ions diffusion is slow, can lead to the preservation of the second phase in the ceramics. Besides, insufficient material plasticity can lead to microcracks in the ceramics when the phase transitions take place. Thus, it is quite difficult to determine in advance whether the $La_2O_3$ can be used as an aid to sinter highly transparent $Ho_2O_3$ ceramics, as well as to predict an optimal concentration of the aid.

The aim of this research is to apply the SHS technique to holmium oxide − lanthana solid solutions as well as to investigate in detail properties of the nanopowders fabricated to determine the possibility of the powders to be used to sinter the highly transparent ceramics for magneto-optical applications.

## 2. Materials and methods

The materials to use for the synthesis of SHS precursors were holmium oxide (99.99% Polirit, Russia), lanthanum oxide (99.99% Polirit, Russia), nitric acid (99.9999%, Khimreaktiv, Russia) and glycine $NH_2CH_2COOH$ (99.9%, Khimreaktiv, Russia). The nanopowders preparation was carried out according to SHS glycine-nitrate method described earlier in detail for other rare-earth metal oxides [1, 2, 25]. Holmium and lanthanum nitrates were prepared by dissolving 10 g of holmium or lanthanum oxide in a stoichiometric amount of the nitric acid upon heating. The concentration of the solutions was determined by a thermogravimetric method after calcining the dry residue at 1200 °C. The nitrates were mixed in a proportion depending on the desired composition of the mixed oxide $(Ho_{1-x}La_x)_2O_3$. The glycine was added to the solution of the metal nitrates in a molar ratio of 1:1 and water was evaporated next at a temperature of about 110 °C. A weighed portion of the precursor in a quartz flask was placed in a furnace preheated to 400 °C where initiation of the SHS redox exothermic reactions and their propagation over the entire sample took place.


https://doi.org/10.1016/j.heliyon.2019.e01519

Grinding of the powders after the SHS was carried out in a ball mill (Labtools, Russia) in polyurethane jar. The yttrium stabilized zirconia balls (YSZ, SiLibeads, SIGMUND LINDNER GmbH, Germany) with a diameter of 5 mm and absolute isopropyl alcohol, which was purified by distillation at atmospheric pressure, were used. The grinding was carried out for 72 hours at a rotation speed of 240 rpm. The obtained suspension was separated from the grinding balls on a sieve with a mesh size of 355 μm. Next, the suspension in 25 ml centrifuge tubes was treated in a laboratory centrifuge (OPN-8, Russia) for 5 minutes at a rotation speed of 3000 rpm (about 800 g). The centrifugate was separated by decantation, dried in a drying oven at 80 °C and calcined in air in a muffle furnace at 700 °C for 5 hours, to remove residual alcohol.

Phase structure and composition of the nanopowders were characterized with powder X-ray diffraction (XRD). The XRD was recorded with a D8 DISCOVER GADDS (Bruker AXS, Germany) with Cu ($K_{\alpha 1,2}$ $\lambda = 1{,}542$ Å) radiation and a carbon monochromator. The XRD data were analyzed using the TOPAS 3 software (Bruker AXS, Germany) with Rietveld's algorithm to specify structure parameters. The particle size was calculated using Scherrer's method [42] regarding diffraction line broadening (compensation factor $k = 0.89$). Theoretical density of the solid solution was calculated from the results of XRD analysis according to formula (1) [43]:

$$\rho_{XRD} = \frac{Z \times M}{V \times N_A}, \tag{1}$$

where $Z$ is a number of structural units in the unit cell (16 for the cubic crystal structure of bixbyite), $M$ – average molar mass, $V$ – the unit cell volume, $N_A$ – Avogadro's number.

The specific surface area ($S_{\mathrm{BET}}$) of the nanopowders was measured by nitrogen adsorption according to the BET method [44] (TriStar 3000, Micromeritics, USA). If the particles are assumed to be spherical, the average diameter of spherical particles can be calculated in accordance with Eq. (2):

$$d_{BET} = \frac{6}{\rho S_{BET}}, \tag{2}$$

where $S_{BET}$ is the specific surface area of the powder, and $\rho$ the density of the material.

Adsorbates content and exo/endothermal reactions that take place during annealing at up to 1400 °C were analyzed by simultaneous thermal analysis (TG-DSC) with a NETZSCH-STA409PC (NETZSCH, Germany). Particle size and morphology were investigated by scanning electron microscopy (SEM) (AURIGA CrossBeam, Carl Zeiss NTS, Germany). Fourier-transform infrared (FT-IR) spectra of the nanopowders were monitored with a FT-IR Spectrometer Tenzor-27 (Bruker, USA). For this,


https://doi.org/10.1016/j.heliyon.2019.e01519

the powders were mixed with KBr in ratio 3:1000 and compacted to a pellet at 500 MPa.

The particle size distribution was measured by a dynamic light scattering (DLS) method with NanoBrook 90Plus Zeta (Brookhaven Instruments Corporation, USA) equipment. To do this, suspensions of 0.1 g of the nanopowders in 20 ml of isopropyl alcohol with the addition of Triton-X 100 (laboratory grade, Sigma-Aldrich, USA) surfactant to stabilize the particles were prepared.

## 3. Results and discussion

A study of the morphology of the SHS powders carried out with scanning electron microscopy showed that, prior to annealing and grinding, the powder is a typical SHS product – a mixture of nanoparticles with a size of about 20 nm (primary particles) and large spongy particles (pieces of a solidified foam) ranging in size from hundreds of nanometers (Fig. 1a) to tens of micrometers with a developed surface area. These large particles were not taken in the picture (Fig. 1a) for the sake of magnification, but their internal structure is similar to one shown in Fig. 1c. This structure of the SHS powder ensues from the mechanism of the synthesis. With the propagation of the reaction front, the precursor foams up at first and only then the combustion reaction starts, proceeding with a release of a large amount of gaseous products. In general, such morphology of the powder is quite undesirable in the case of optical ceramics sintering, since the coarse spongy structured particles tend to form density gradients and voids in a green body upon compaction.

After annealing of the powder at 700 °C in air, ball milling and sedimentation in a centrifuge, the powder became more homogeneous, particles larger than 200–300 nm were not observed (Fig. 1b). The portion of coarse particles (larger than 300 nm) separated by the centrifugation from the nanoparticles was less than 10 wt.%. The primary particles are irregularly shaped and their size is less than 20 nm. Large particles, which were precipitated during the sedimentation, held the spongy structure with a developed surface (Fig. 1c).

A significant change of the morphology of both the primary particles and the sediment happens when the powder is annealed at 900 °C. Primary particles rounded (Fig. 1d), still with certain edges, which are caused by the crystallization of the SHS particles upon annealing. The large particles precipitated during the centrifugation differ much more drastically (Fig. 1e). The large particles lose their spongy structure and turn into agglomerates (secondary particles) with a characteristic size of more than 200 nm. The degree of bonding of the primary particles in such agglomerates differs among the secondary ones. Some of the secondary particles have a fairly strong polycrystalline structure; others consist of loosely bounded


https://doi.org/10.1016/j.heliyon.2019.e01519

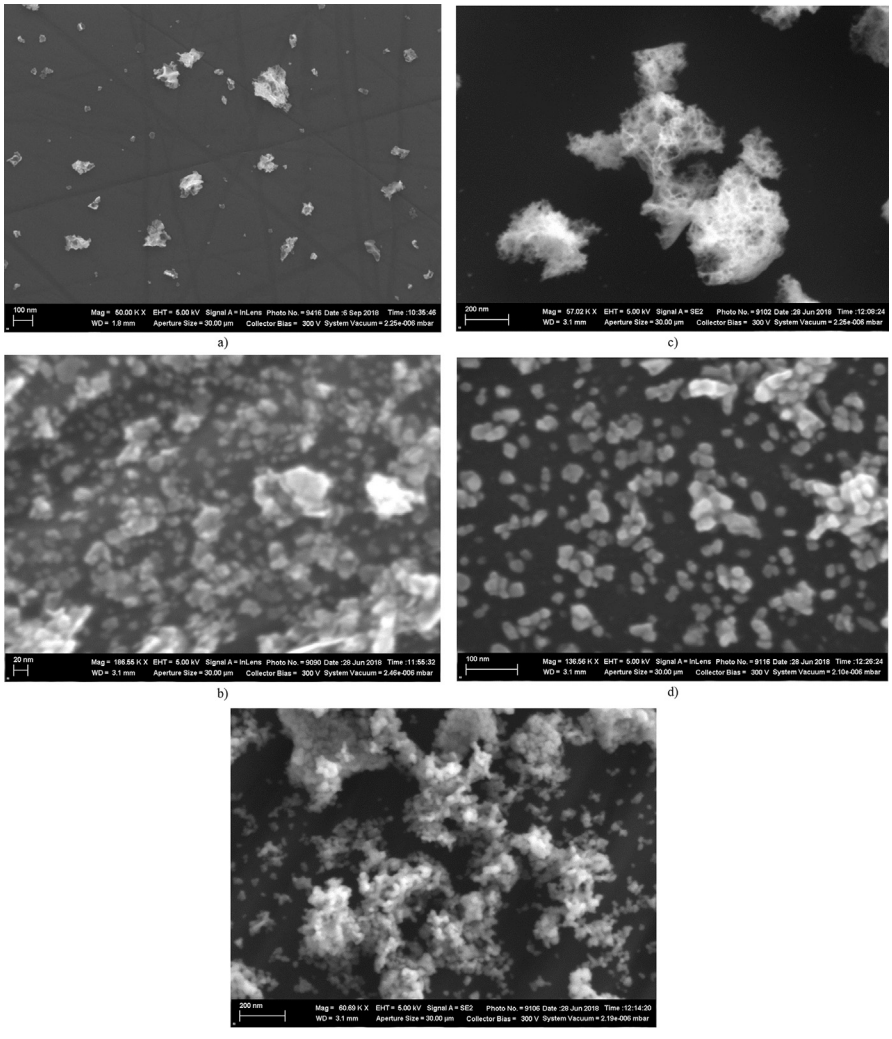


**Fig. 1.** Micrographs of the $(Ho_{1-x}La_x)_2O_3$ powders prepared by the SHS method: (a) as made, (b) nanoparticles and (c) sediment after annealing at 700 °C, ball milling and sedimentation and (d) nanoparticles and (e) sediment after annealing at 900 °C, ball milling and sedimentation.


https://doi.org/10.1016/j.heliyon.2019.e01519

primary particles, which can be easily deagglomerated by a mild treatment in an ultrasonic bath.

Fig. 2 shows the size distributions of the particles after the ball milling measured by the dynamic light scattering method. The distributions are in a good agreement with the data of the scanning electron microscopy. The powders consist of two clearly distinguishable fractions - primary particles with a characteristic size of tens of nanometers and agglomerates of particles with an effective diameter of about 200 nm. The primary particles average sizes of both as made and annealed at 700 °C powders are somewhat larger than ones observed in the SEM pictures (Fig. 1), which seems to be caused by the irregular shape of these nanoparticles, since the DLS method measures the largest dimension size due to a chaotic rotation of the particles in the suspension resulting from Brownian motion. The particles annealed at 900 °C acquire a rounded shape and their sizes measured by the DLS nearly coincide with the SEM observation. Paying attention to a large volume fraction of the secondary particles in the distributions (Fig. 2), it should be noted that this data represents the real ratio of the primary and secondary particles in the powder much more accurately in comparison with one conceived from the SEM pictures, since a volume of one particle with size of 100 nm equals in about $10^3$ nanoparticles of 10 nm in size.

In general, it can be concluded that annealing of the SHS $(Ho_{1-x}La_x)_2O_3$ powder at the temperature of about 900 °C in air, subsequent ball milling and sedimentation

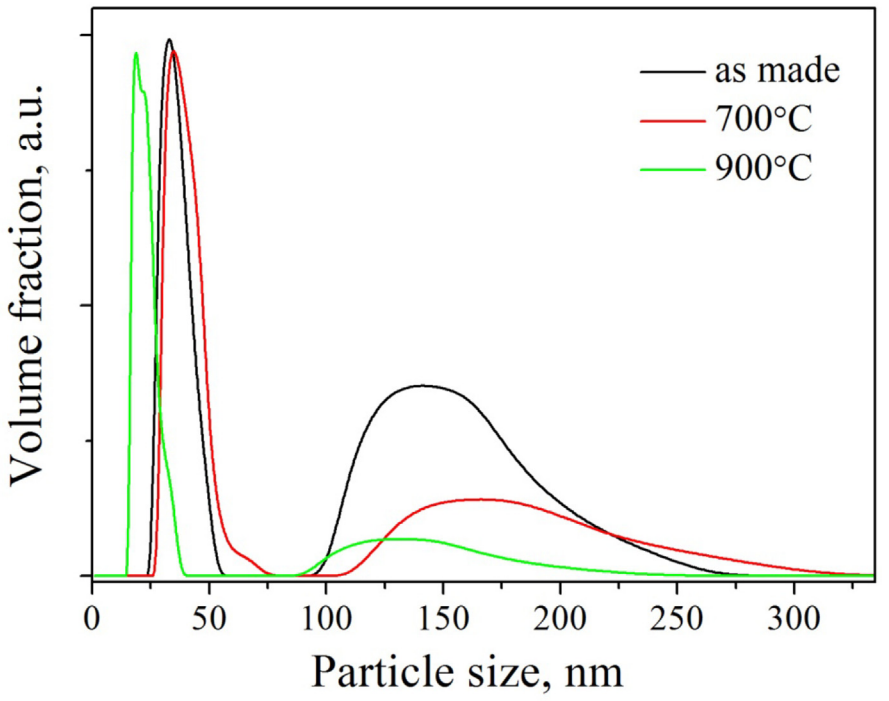


**Fig. 2.** Size distribution of the SHS particles after ball milling: "as made" and annealed at 700 and 900 °C for 3 h.


https://doi.org/10.1016/j.heliyon.2019.e01519

result in the nanopowder which consists of non-agglomerated nanoparticles with a shape close to spherical and the mean size of about 20 nm and loosely bounded (fragile) aggregates of such particles with a mean size of 150−350 nm. Comparing the morphology of the powders to commercial ones commonly used in the optical ceramics sintering [34], one can expect the SHS powder to turn into highly transparent ceramics if compaction and sintering conditions are optimal.

Fig. 3 presents XRD spectra of the $(Ho_{1-x}La_x)_2O_3$ powders prepared by the SHS with the lanthana content from 0 to 10 mol%. It can be seen that, regardless of the powder composition, the peaks are broadened due to the small sizes of the crystallites. The size of the coherence area is given in Table 1. Within limits of the measurement error, the size loosely depends on the solid solution composition and is about 10 nm. The analysis of the X-ray patterns shows that all the powders have a C-type cubic crystal lattice of $RE_2O_3$ sesquioxides (space group Ia-3, No. 206, Z = 16). No secondary phases are observed, which proves the holmium oxide nanopowders prepared by the SHS to dissolve up to 10 mol.% of lanthana. Worth mentioning is a fact that, according to the literature [35, 36], the solubility of the $La_2O_3$ in the cubic holmium oxide matrix has its maximum at temperatures of 1000−1200 °C (about 12 mol.%) and decreases with the temperature decrease. At 500 °C it's approximately 6 mol.%, and at the room temperature it does not exceed 4−6 mol.%. The absence of the second phases in the "as made" $(Ho_{1-x}La_x)_2O_3$ powders at room temperature can be explained by several causes: the small size of the crystallites, the presence of a significant amount of defects in the nanoparticles after synthesis, as well as the

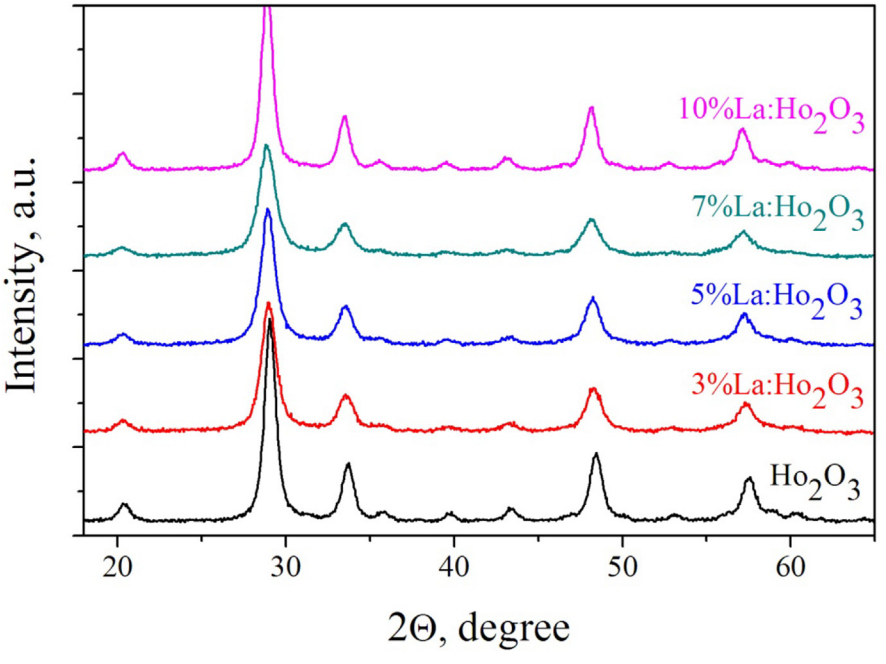


**Fig. 3.** XRD spectra of the "as made" $(Ho_{1-x}La_x)_2O_3$ powders.


https://doi.org/10.1016/j.heliyon.2019.e01519

**Table 1.** Average crystalline size ($d_{XRD}$), lattice parameter (a), theoretical density ($\rho_{XRD}$), specific surface area ($S_{BET}$) and equivalent average particle size ($d_{BET}$) of the "as made" SHS $(Ho_{1-x}La_x)_2O_3$ powders.

| Composition | $d_{XRD}$, nm | a, Å | $\rho_{XRD}$, g/cm$^3$ | $S_{BET}$, m$^2$/g | $d_{BET}$, nm |
|---|---|---|---|---|---|
| $Ho_2O_3$ | 12.5 ± 0.5 | 10.62 ± 0.02 | 8.401 | 31.5 ± 0.1 | 22.7 ± 0.1 |
| $(Ho_{0.97}La_{0.03})_2O_3$ | 8.6 ± 0.5 | 10.65 ± 0.02 | 8.273 | 30.5 ± 0.1 | 23.8 ± 0.1 |
| $(Ho_{0.95}La_{0.05})_2O_3$ | 8.6 ± 0.5 | 10.66 ± 0.02 | 8.227 | 38.1 ± 0.1 | 19.1 ± 0.1 |
| $(Ho_{0.93}La_{0.07})_2O_3$ | 7.2 ± 0.5 | 10.68 ± 0.02 | 8.158 | 25.1 ± 0.1 | 29.3 ± 0.1 |
| $(Ho_{0.9}La_{0.1})_2O_3$ | 12 ± 1 | 10.69 ± 0.02 | 8.101 | 36.0 ± 0.1 | 20.6 ± 0.1 |

freezing of a structure of the solid solution formed in the region of 1000 °C (which corresponds to the flow temperature of the SHS). However surprisingly, in the powders calcined at a temperature of 1400 °C for 3 h none of the second phases segregated either, even in the $(Ho_{0.9}La_{0.1})_2O_3$ composition, in spite of a significant increase in the crystallite size up to 260−280 nm.

The absence of the segregation was additionally confirmed by a dependence of the $Ho_2O_3$ cubic phase lattice parameter on the lanthana content, which corresponds to the Vegard's law (Fig. 4) both in the case of the annealed at 1400 °C and the "as made" $(Ho_{1-x}La_x)_2O_3$ powders. A larger ionic radius of $La^{3+}$ (1.061 Å) in comparison with $Ho^{3+}$ (0.894 Å) should lead to an increase of the $Ho_2O_3$ lattice parameter with the lanthana content. Given the accuracy of the measurement, in the case of the

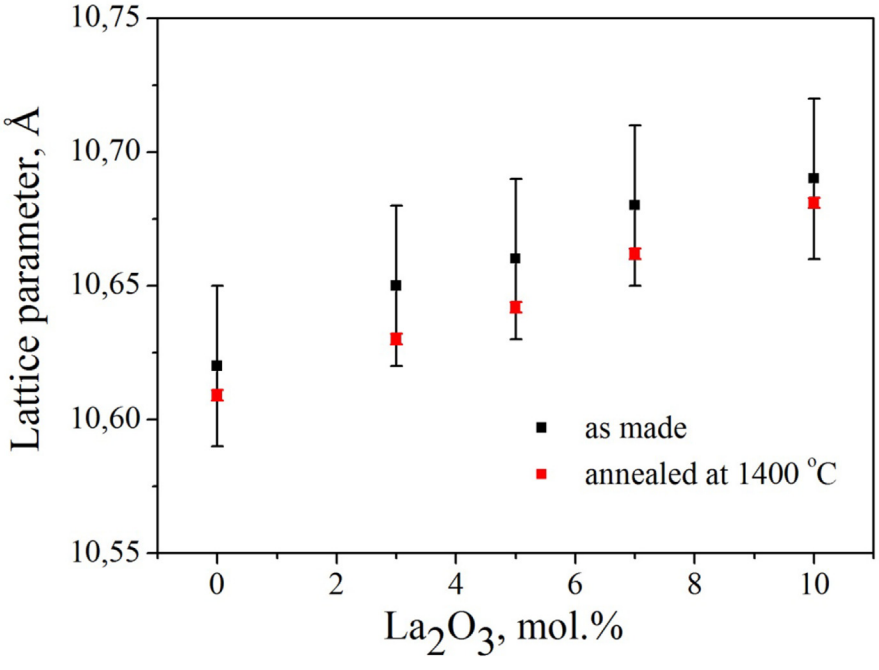


**Fig. 4.** Dependence of the $Ho_2O_3$ cubic phase lattice parameter on the lanthana content.


https://doi.org/10.1016/j.heliyon.2019.e01519

"as made" nanopowders the dependence is concealed, which is caused by the broadening of the XRD peaks due to the small crystallite sizes. In the case of the annealed powders, the margin of error is 10 times smaller (±0.003 Å, not shown in the graph for the small value) and the dependence is clearly linear up to 10 mol.% of lanthana that confirm the amount to be soluble in the $Ho_2O_3$ nanoparticles.

Using the values of the lattice parameter $a$, a theoretical density of the $(Ho_{1-x}La_x)_2O_3$ solid solutions was estimated and the equivalent particle diameters $d_{BET}$ were calculated from the specific surface $S_{BET}$ of the powders. The values of the specific surface of the powders and the equivalent particle diameter are given in Table 1. Taking in account a fact that the primary particles of the "as made" SHS powders are irregularly shaped and the secondary particles have a sponge structure with a highly developed surface, there's a little wonder to find out the $d_{BET}$ calculated on the nanoparticle's spherical shape assumption to be smaller than the particles' actual size. Worth mentioning is a slight variation of the $S_{BET}$, which is not related to the powders elemental composition. We believe the differences to be caused by the secondary particles' closed porosity since the surface inside the pores is not measured by the BET method. The value of the closed porosity varies quite randomly due to a certain inaccuracy of both the measurement of an oxidant − fuel ratio at the precursor preparation stage and a slight variation of the temperature in the reaction zone during the SHS. The calcination and ball milling of the SHS powders lead to both rupture of the secondary particles' sponge structure and smoothing the shape of the primary particles. After the annealing and grinding, the SEM and DLS measurements (Figs. 1 and 2) give the data on the particles sizes which are in a reasonable agreement with each other. Nevertheless, the $S_{BET}$ of the powders of any compositions after the calcination at 900 °C and ball milling are about 19 $m^2/g$ that means the $d_{BET}$ is about 40 nm.

With the view of finding out the behavior of the nanopowders during compaction and sintering, an important issue is to evaluate the content of any intermediate products of the redox reactions, adsorbed gases and water as well as to find a way to eliminate them. Fig. 5 shows data of the simultaneous thermal analysis of the $(Ho_{0.95}La_{0.05})_2O_3$ powders prepared by SHS. According to the thermogravimetry data, when the powder is heated up to a temperature of about 950 °C, its mass decreases by 6.7%. The main substance desorbed during the heating up to 900 °C is $H_2O$. At the temperatures of about 200−400 and 550−800 °C the spectrum reveals a small amount of $CO_2$. A release of NO was detected at 200−350 and 450−700 °C. A release of $NO_2$ was not detected upon heating. The presence of water and carbon dioxide in the nanopowder is easily explained since they are not only the main products of the SHS reaction but can also be quickly adsorbed from the air due to the developed surface of the nanopowder [37, 38]. The presence of nitrogen oxides in the powder is due to the SHS process in an excess of the oxidizing agent (holmium nitrate). The absence of pronounced peaks on the TG/DSC curves reflects the


https://doi.org/10.1016/j.heliyon.2019.e01519

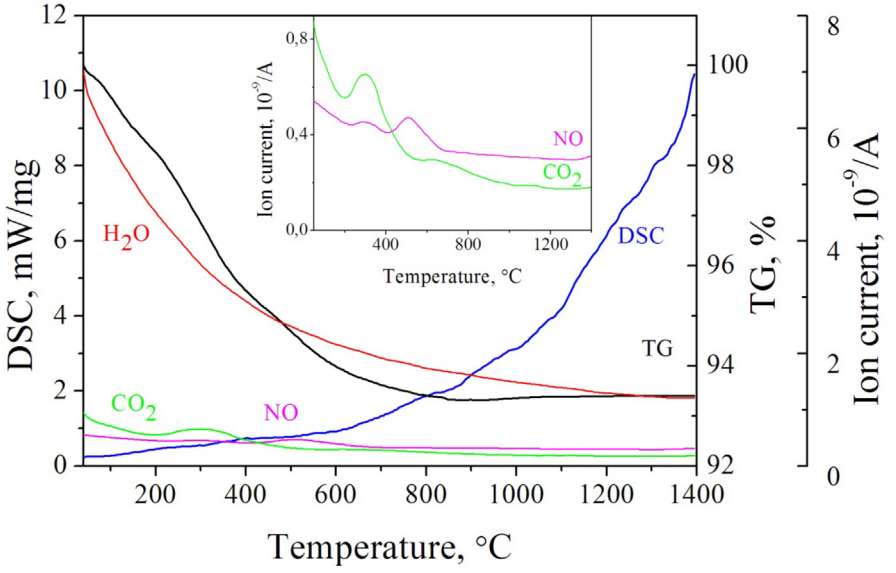


**Fig. 5.** TG/DSC curves of the "as made" $(Ho_{0.95}La_{0.05})_2O_3$ nanopowder. Panel inserted – desorbed gases mass spectrometry data.

insignificant content of unreacted precursors or intermediates in the SHS powder as well as the absence of any phase transitions up to a temperature of 1400 °C.

The FT-IR analysis (Fig. 6) confirmed the presence of $OH^-$, $CO_3^{2-}$ and $NO_3^-$ in the $(Ho_{0.95}La_{0.05})_2O_3$ nanopowders. The absorption bands observed in the spectra and chemical substances corresponding to the bands are shown in Table 2. Since the nanopowders have a developed surface, they absorb a considerable amount of water. The water molecules interact strongly with the surface of the nanoparticles and form hydroxide layers. Consecutively, the alkaline surface layer of the holmium reacts with $CO_2$ also adsorbed from the air and forms carbonates. Evidence of nitrate ($NO_3^-$) formation in the as made powders could be found as peaks at 1384 $cm^{-1}$, 1055 $cm^{-1}$ and 841 $cm^{-1}$, assigned to $D_{3h}$ point group $v_3(E')$, $v_1(A_1')$ and $v_2(A_2'')$ vibrations respectively [39], but in this spectrum the last two are overridden by the $CO_3^{2-}$ absorption. The formation of the nitrate groups is associated with the presence of the products of the SHS reaction (water and nitrogen oxides) in the pores of the secondary particles, which form nitric acid and then holmium nitrate.

After calcination of the nanopowders in the air at temperatures of about 700–900 °C and cooling down no nitrates were detected by the FT-IR. Nevertheless, the powders readily adsorbed $H_2O$ and $CO_2$ and formed a significant amount of hydroxide and carbonates (Fig. 6). A similar process was observed in the case of yttria particles with a developed surface [40]. Considering the nanopowders to be quite a promising starting material to sinter transparent ceramics, one should pay attention to the recurring formation of the carbonates in the calcined nanopowders exposed to air. At a stage of vacuum sintering of the powder, an impurity phase can be formed due to


https://doi.org/10.1016/j.heliyon.2019.e01519

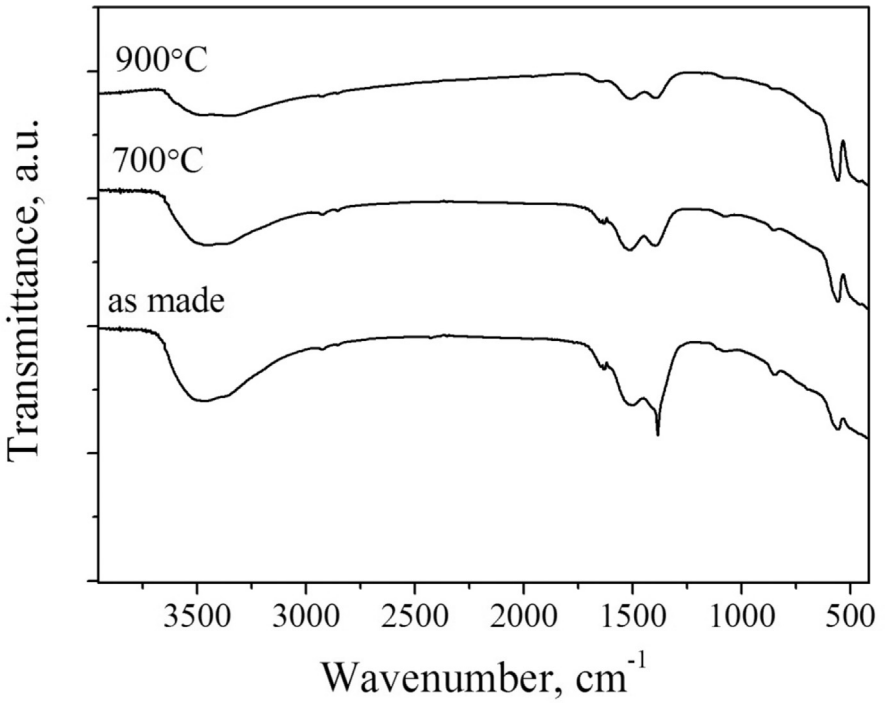


**Fig. 6.** FT-IR spectra (KBr disks) of the $(Ho_{0.95}La_{0.05})_2O_3$ nanopowder obtained from the SHS: "as made" and calcined in air at 700 and 900 °C for 3 h.

**Table 2.** FT-IR analysis of the $(Ho_{1-x}La_x)_2O_3$ nanopowder.

| Maximum of absorption band, $cm^{-1}$ | Assignments [41] |
|---|---|
| 3700−3000 | $OH^-$ stretch |
| 1650−1630 | H−O−H bend ($\nu_2$) |
| 1515 | $CO_3^{2-}$ $\nu_3$ asymmetric stretch |
| 1398 | $CO_3^{2-}$ $\nu_3$ symmetric stretch |
| 1384 (narrow) | $NO_3^-$ symmetric stretch |
| 1077 | $CO_3^{2-}$ $\nu_1$ symmetric stretch |
| 847 | $CO_3^{2-}$ $\nu_2$ out-of-plane deformation |
| 556 | Ho−O lattice vibration |

the carbon, which severely damages transparency of the ceramics. Thus, certain precautions should be taken to prevent adsorption of the wet air by the powders and compacts before sintering.

## 4. Conclusions

Synthesis of the $(Ho_{1-x}La_x)_2O_3$ powder with the help of the self-propagating high-temperature synthesis, subsequent annealing at 900 °C in air, ball milling and


https://doi.org/10.1016/j.heliyon.2019.e01519

sedimentation give a chance to obtain the nanopowder, which consists of nearly spherical non-agglomerated nanoparticles with a characteristic size of about 20 nm and weakly bounded (fragile) agglomerates of the particles with a characteristic size of 150−350 nm. The $(Ho_{1-x}La_x)_2O_3$ nanoparticles have a C-type cubic crystal structure. Up to 10 mol.% of the lanthana can be dissolved in the holmium oxide nanopowder. No second phases were detected. The "as made" $(Ho_{1-x}La_x)_2O_3$ powder was found to contain water, carbonates and nitrates in an amount of about 7 wt.%. Annealing of the powder at 900 °C for 3 h decreases the specific surface area to a half and eliminates the nitrates. Exposing of the annealed powder to the humid air leads to adsorption of the water and carbon dioxide and recurring formation of the carbonates, which should be taken in account when the powder is used to make optical ceramics.

## Declarations

### Author contribution statement

S. S. Balabanov, M. G. Ivanov: Conceived and designed the experiments; Analyzed and interpreted the data; Wrote the paper.

S. V. Filofeev, E. G. Kalinina, D. K. Kuznetsov, E. Y. Rostokina: Performed the experiments.

D. A. Permin: Performed the experiments; Analyzed and interpreted the data.

### Funding statement

This work was supported by the Russian Science Foundation (research project No. 18-13-00355).

### Competing interest statement

The authors declare no conflict of interest.

### Additional information

No additional information is available for this paper.

## References

[1] S.S. Balabanov, D.A. Permin, E.Y. Rostokina, S.V. Egorov, A.A. Sorokin, D.D. Kuznetsov, Synthesis and structural characterization of ultrafine terbium oxide powders, Ceram. Int. 43 (2017) 16569−16574.


https://doi.org/10.1016/j.heliyon.2019.e01519

[2] I.L. Snetkov, D.A. Permin, S.S. Balabanov, O.V. Palashov, Wavelength dependence of Verdet constant of $Tb^{3+}$:$Y_2O_3$ceramics, Appl. Phys. Lett. 108 (2016).

[3] H. Furuse, R. Yasuhara, Magneto-optical characteristics of holmium oxide ($Ho_2O_3$) ceramics, Opt. Mater. Express 7 (2017) 827.

[4] D. Vojna, R. Yasuhara, H. Furuse, O. Slezak, S. Hutchinson, A. Lucianetti, T. Mocek, M. Cech, Faraday effect measurements of holmium oxide ($Ho_2O_3$) ceramics-based magneto-optical materials, High Power Laser Sci. Eng. 6 (2018) e2.

[5] P. Veber, M. Vel?zquez, G. Gadret, D. Rytz, M. Peltz, R. Decourt, Flux growth at 1230C of cubic $Tb_2O_3$ single crystals and characterization of their optical and magnetic properties, CrystEngComm 17 (2015) 492−497.

[6] A. Yakovlev, I. Snetkov, D. Permin, S. Balabanov, O. Palashov, Faraday rotation in cryogenically cooled dysprosium based ($Dy_2O_3$) ceramics, Scr. Mater. 161 (2019) 32−35.

[7] I.L. Snetkov, A.I. Yakovlev, D.A. Permin, S.S. Balabanov, O.V. Palashov, Magneto-optical Faraday effect in dysprosium oxide ($Dy_2O_3$) based ceramics obtained by vacuum sintering, Opt. Lett. 43 (2018) 4041.

[8] K. Kendall, Influence of powder structure on processing and properties of advanced ceramics, Powder Technol. 58 (1989) 151−161.

[9] M. Ivanov, Y. Kopylov, V. Kravchenko, J. Li, A. Medvedev, Y. Pan, Highly transparent ytterbium doped yttrium lanthanum oxide ceramics, J. Rare Earths 32 (2014) 254−258.

[10] S. Li, X. Zhu, J. Li, R. Yavetskiy, M. Ivanov, B. Liu, W. Liu, Y. Pan, Fabrication of 5 at.%Yb:(La 0.1 Y 0.9 ) $2O_3$ transparent ceramics by chemical precipitation and vacuum sintering, Opt. Mater. 71 (2017) 56−61.

[11] B. Liu, J. Li, R. Yavetskiy, M. Ivanov, Y. Zeng, T. Xie, H. Kou, S. Zhuo, Y. Pan, J. Guo, Fabrication of YAG transparent ceramics using carbonate precipitated yttria powder, J. Eur. Ceram. Soc. 35 (2015) 2379−2390.

[12] M.G. Ivanov, Y.L. Kopylov, V.B. Kravchenko, K.V. Lopukhin, V.V. Shemet, YAG and $Y_2O_3$ laser ceramics from nonagglomerated nanopowders, Inorg. Mater. 50 (2014) 951−959.

[13] I.S. Puzyrev, I.V. V'yukhina, M.G. Ivanov, Y.G. Yatluk, Development of methods for preparation of Nd: YAG nanoparticles, Glas. Phys. Chem. 38 (2012) 427−430.


https://doi.org/10.1016/j.heliyon.2019.e01519

[14] M. Ivanov, E. Kalinina, Y. Kopylov, V. Kravchenko, I. Krutikova, U. Kynast, J. Li, M. Leznina, A. Medvedev, Highly transparent Yb-doped (La x Y 1−x ) $2O_3$ ceramics prepared through colloidal methods of nanoparticles compaction, J. Eur. Ceram. Soc. 36 (2016) 4251−4259.

[15] D.A. Permin, S.V. Kurashkin, A.V. Novikova, A.P. Savikin, E.M. Gavrishchuk, S.S. Balabanov, N.M. Khamaletdinova, Synthesis and luminescence properties of Yb-doped $Y_2O_3$, $Sc_2O_3$ and $Lu_2O_3$ solid solutions nanopowders, Opt. Mater. 77 (2018) 240−245.

[16] D.A. Permin, A.V. Novikova, E.M. Gavrishchuk, S.S. Balabanov, A.A. Sorokin, Self-propagating high-temperature synthesis of $Lu_2O_3$ powders for optical ceramics, Inorg. Mater. 53 (2017) 1330−1335.

[17] S.S. Balabanov, Y.V. Bykov, S.V. Egorov, A.G. Eremeev, E.M. Gavrishchuk, E.A. Khazanov, I.B. Mukhin, O.V. Palashov, D.A. Permin, V.V. Zelenogorsky, Transparent Yb:$(YLa)_2O_3$ceramics produced by self-propagating high-temperature synthesis and microwave sintering, Opt. Mater. 35 (2013).

[18] S.S. Balabanov, E.M. Gavrishchuk, D.A. Permin, Y.V. Bykov, S.V. Egorov, A.G. Eremeev, E.A. Khazanov, I.B. Mukhin, O.V. Palashov, V.V. Zelenogorskii, Yb: $(YLa)_2O_3$ laser ceramics produced by microwave sintering, Quantum Electron. 43 (2013).

[19] S.S. Balabanov, E.M. Gavrishchuk, A.M. Kut'in, D.A. Permin, Self-propagating high-temperature synthesis of $Y_2O_3$ powders from $Y(NO_3)3x$ $(CH_3COO)_3(1-x)…nH_2O$, Inorg. Mater. 47 (2011) 484−488.

[20] N. Wang, X. Zhang, Z. Bai, Q. Liu, L. Lu, X. Mi, H. Sun, X. Wang, Carbonate-precipitation synthesis of Yb3+:$Y_2O_3$ nanopowders and its characteristics, Powder Technol. 203 (2010) 458−461.

[21] M. Ivanov, Y. Kopylov, V. Kravchenko, S. Zayats, Sintering and optical quality of highly transparent yb-doped yttrium lanthanum oxide ceramics, Phys. Status Solidi 10 (2013) 940−944.

[22] Y.A. Kotov, V.V. Osipov, M.G. Ivanov, O.M. Samatov, V.V. Platonov, V.V. Lisenkov, A.M. Murzakayev, A.I. Medvedev, E.I. Azarkevich, A.K. Shtolz, O.R. Timoshenkova, Properties of YSZ and CeGdO nanopowders prepared by target evaporation with a pulse-repetitive $CO_2$-laser, Rev. Adv. Mater. Sci. 5 (2003) 171−177.

[23] Y.A. Kotov, V.V. Osipov, O.M. Samatov, M.G. Ivanov, V.V. Platonov, A.M. Murzakaev, E.I. Azarkevich, A.I. Medvedev, A.K. Shtolts, O.R. Timoshenkova, Properties of powders produced by evaporating $CeO_2$/

 https://doi.org/10.1016/j.heliyon.2019.e01519

$Gd_2O_3$ targets exposed to pulsed-periodic radiation of a $CO_2$ laser, Tech. Phys. 49 (2004) 352−357.

[24] Y.A. Kotov, O.M. Samatov, M.G. Ivanov, A.M. Murzakaev, A.I. Medvedev, O.R. Timoshenkova, T.M. Demina, I.V. V'yukhina, Production and characteristics of composite nanopowders using a fiber ytterbium laser, Tech. Phys. 56 (2011) 652−655.

[25] D.A. Permin, S.S. Balabanov, A.V. Novikova, I.L. Snetkov, O.V. Palashov, A.A. Sorokin, M.G. Ivanov, Fabrication of Yb-doped $Lu_2O_3$-$Y_2O_3$-$La_2O_3$ solid solutions transparent ceramics by self-propagating high-temperature synthesis and vacuum sintering, Ceram. Int. (2018).

[26] W.H. Rhodes, Controlled transient solid second-phase sintering of yttria, J. Am. Ceram. Soc. 64 (1981) 13−19.

[27] I.L. Snetkov, I.B. Mukhin, S.S. Balabanov, D.A. Permin, O. V Palashov, Efficient lasing in Yb:$(YLa)_2O_3$ ceramics, Quantum Electron. 45 (2015) 95−97.

[28] A. Ikesue, I. Furusato, K. Kamata, Fabrication of polycrystal line, transparent YAG ceramics by a solid-state reaction method, J. Am. Ceram. Soc. 78 (1995) 225−228.

[29] Q. Liu, J. Liu, J. Li, M. Ivanov, A. Medvedev, Y. Zeng, G. Jin, X. Ba, W. Liu, B. Jiang, Y. Pan, J. Guo, Solid-state reactive sintering of YAG transparent ceramics for optical applications, J. Alloys Compd. 616 (2014) 81−88.

[30] S.S. Balabanov, E.M. Gavrishchuk, E.Y. Rostokina, A.D. Plekhovich, V.N. Kuryakov, S.V. Amarantov, N.M. Khamaletdinova, R.P. Yavetskiy, Colloid chemical properties of binary sols as precursors for YAG optical ceramics, Ceram. Int. 42 (2016).

[31] S.S. Balabanov, E.M. Gavrishchuk, V.V. Drobotenko, O.V. Palashov, E.Y. Rostokina, R.P. Yavetskiy, A new approach to $Y_3Al_5O_{12}$ transparent ceramics by vacuum sintering of spray-dried xerogels, Ceram. Int. 42 (2016).

[32] B. Liu, J. Li, M. Ivanov, W. Liu, L. Ge, T. Xie, H. Kou, S. Zhuo, Y. Pan, J. Guo, Diffusion-controlled solid-state reactive sintering of Nd:YAG transparent ceramics, Ceram. Int. 41 (2015) 11293−11300.

[33] J. Liu, X. Cheng, J. Li, T. Xie, M. Ivanov, X. Ba, H. Chen, Q. Liu, Y. Pan, J. Guo, Influence of non-stoichiometry on solid-state reactive sintering of YAG transparent ceramics, J. Eur. Ceram. Soc. 35 (2015) 3127−3136.

[34] L. Esposito, A. Piancastelli, Role of powder properties and shaping techniques on the formation of pore-free YAG materials, J. Eur. Ceram. Soc. 29 (2009) 317−322.

 https://doi.org/10.1016/j.heliyon.2019.e01519

[35] M. Zinkevich, Thermodynamics of rare earth sesquioxides, Prog. Mater. Sci. 52 (2007) 597−647.

[36] Y. Zhang, Thermodynamic Properties of Rare Earth Sesquioxides, McGill University Libraries, 2017.

[37] I.S. Puzyrev, M.G. Ivanov, I.V. Krutikova, Physicochemical properties of $Al_2O_3$ and $Y_2O_3$ nanopowders produced by laser synthesis and their aqueous dispersions, Russ. Chem. Bull. 63 (2014) 1504−1510.

[38] M.G. Ivanov, U. Kynast, M. Leznina, Eu3+ doped yttrium oxide nano-luminophores from laser synthesis, J. Lumin. 169 (2016) 744−748.

[39] R. Kato, J. Rolfe, Vibration frequencies of NO2− and NO3− ions in KBr crystals, J. Chem. Phys. 47 (1967) 1901−1910.

[40] M.G. Ivanov, I.V. Krutikova, U. Kynast, M. Lezhnina, I.S. Puzyrev, Laser-synthesized $Y_2O_3$:Eu3+ nanophosphors and their stabilization in water suspensions, Opt. Mater. 74 (2017) 67−75.

[41] K.D.J. Weidlein, U. Müller, Schwingungsfrequenzen I. Hauptgruppenelemente,, Georg Thieme Verlag Stuttgart, New York, 1981.

[42] A. Patterson, The Scherrer formula for X-ray particle size determination, Phys. Rev. 56 (10) (1939) 978−982.

[43] William G. Schlecht, Calculation of density from X-ray data, Am. Mineral. 29 (1944) 108−110.

[44] S. Brunauer, P. Emmett, E. Teller, Adsorption of gases in multimolecular layers, J. Am. Ceram. Soc. 60 (2) (1938) 309−319.


https://doi.org/10.1016/j.heliyon.2019.e01519